Liquid-Gas Phase Transition of Supernova Matter and Its Relation to Nucleosynthesis ⋆

C. Ishizuka [a], A. Ohnishi [a] and K. Sumiyoshi [b]

[a] *Division of Physics, Graduate School of Science, Hokkaido University, Sapporo 060-0810, Japan*

[b] *Numazu College of Technology, Numazu 410-8501, Japan*

Abstract

We investigate the liquid-gas phase transition of dense matter in supernova explosion systematically from $\rho_B = 10^{-10}$ to 10^{-1} fm^{-3} by using a relativistic mean field approach and a fragment based statistical model. The boiling temperature is determined and found to remain to be high for low density. Calculated fragment distribution shows that heavy elements around the first, second, and third peaks of r-process are abundantly formed as the baryon density increases at around the boiling temperatures inside the ν-sphere. At around the boiling temperature, various mass elements are formed even outside of the ν-sphere. These results suggest that the statistical distribution effects of fragment configurations in the coexisting region should be treated more carefully in the supernova explosion.

Key words: Liquid-gas phase transition, Supernova explosion, Nucleosynthesis, Equation of state, Relativistic mean field, Nuclear statistical equilibrium
PACS: 26.30.+k, 26.45.+h, 25.70.Pq, 21.65.+f 26.20.+f, 25.70.-z, 26.60.+c,

1 Introduction

It is generally believed that there exist several phases in nuclear matter. Among the phase transitions between these phases, the nuclear liquid-gas phase transition has been extensively studied in these three decades [1]. It takes place in relatively cold (T_{boil} = (5-8) MeV) and less dense ($\rho_B \sim \rho_0/3$) nuclear matter, and it causes multifragmentation in heavy-ion collisions. When

⋆ Published in Nucl. Phys. A **723** (2003), pp 517-543 [arXiv:nucl-th/0208020]

the expanding nuclear matter cools down and goes across the boundary of coexisting region, it becomes unstable against small fluctuations of density or proton fraction, then various fragments are abundantly formed almost simultaneously. Especially at around the critical point, fragment distribution is expected to follow the power law [2], $Y_f \propto A^{-\tau}$, which is one of the characteristic features of critical phenomena. Recent theoretical model studies [3–7] have shown that it is very difficult to describe this fragment distribution in a picture of sequential binary decays of one big compound nucleus, which has been successfully applied to the decay of nuclei at low excitation. This finding suggests that it is necessary to consider *statistical ensemble of various fragment configurations* rather than one dominant configuration in describing fragment formation at around the boundary of coexisting region.

In the universe, the temperature and density of this liquid-gas phase transition would be probed during supernova explosion. In the collapse and bounce stages of supernova explosion, the density and temperature are high enough to keep statistical equilibrium [8,9]. Especially when the neutrino mean free path is sufficiently short, neutrinos are trapped in dense matter. This leads to an approximate conservation of lepton fraction $Y_L = L/B$ and entropy per baryon S/B, where L and B denote the lepton and baryon numbers, respectively. After the core bounce, supernova matter, which is composed of nucleons, leptons and photons, expands and cools down. As the baryon density and the temperature decrease, charged particle reaction rates become insufficient and the chemical equilibrium ceases to hold, namely the system freezes out at this point. If the supernova matter goes across the boundary of coexisting region and the boiling point T_{boil} of the liquid-gas phase transition is higher than the freeze-out temperature T_{fo}, this matter will dissolve into fragments and form various nuclei in a critical manner before freeze-out. It further keeps equilibrium and expands to the freeze-out point. The statistical distribution of fragments at freeze-out would provide the initial condition for following nucleosynthesis such as the r-process. (See following references on r-process [10–14] and references therein.)

The importance of the nuclear liquid-gas phase transition in supernova explosion was already noticed and extensively studied before [16]. However, there are two more points which we should consider further. First, the main interest in the previous works was limited to the modification of the equation of state (EoS). The nuclear distribution as an initial condition for the r-process was not studied well. Secondly, in constructing the EoS of supernova matter, the mean field treatment was applied in which one assumed one kind of large nucleus surrounded by nucleon and alpha gas [17,18]. At temperature much above or below the boiling point, fragment mass distribution is narrow and the one species approximation works well. However, since fluctuation dominates at around the boiling point, it is necessary to take account of fragment mass and isotope distribution. This distribution of fragments can modify the

following r-process nucleosynthesis provided that the freeze-out point is not far from the boiling point.

In this work, we study nuclear fragment formation through the nuclear liquid-gas phase transition during supernova explosion. In order to pursue this possibility quantitatively, it is necessary to determine the liquid-gas coexisting region. We find that the liquid-gas coexisting region extends down to very low density keeping the boiling point around $T_{boil} \sim 1$ MeV in a two-phase coexistence treatment of EoS with the Relativistic Mean Field (RMF) model [17,20–23]. Adiabatic paths of dense matter are found to go through the calculated liquid-gas coexisting region even with high entropy. Having this finding of the passage through the coexisting region, we investigate the fragment distribution at around the boiling point in a statistical model of fragments [4–7], referred to as the Nuclear Statistical Equilibrium (NSE) in astrophysics. We show that heavy elements around the iron, first, second, and third peaks of r-process are abundantly formed with temperatures around and just below T_{boil} in NSE (inside the liquid-gas coexisting region) at densities where neutrinos are approximately degenerated, $\mu_L = \mu_\nu > T$. Calculated isotope distribution of these elements coincides with that in the solar system. We find that it is important to take account of the Coulomb energy reduction from the screening by electrons in dense supernova matter. Outside of ν-sphere, a variety of nuclei with A$\simeq 30 - 80$ appear as frequently as iron peak nuclei and this trend is not very sensitive to proton fraction. In this case, we can also see the specific feature for temperature dependence of the fragment mass distribution around the boiling point.

This paper is organized as follows. We describe the treatment of two-phase coexistence with RMF model in Sec. 2. The liquid-gas coexistence is shown in the (ρ_B, T) diagram. We demonstrate that it would be possible for a part of ejecta in supernova explosion to experience the liquid-gas coexisting region. The effects of liquid-gas coexistence on EoS, proton fraction, and adiabatic path are also studied. In Sec. 3, we describe the nuclear statistical model of fragments at equilibrium (NSE) to study the production of elements. We take into account the Coulomb energy modification from electron screening. We evaluate the fragment distribution at around the boiling point and in the coexisting region within this statistical model. We find that fragments are formed abundantly even at very low densities if the temperature is around the boiling point. We compare the calculated fragment mass and isotope distributions with the solar abundance [25]. In Sec. 4, we discuss the distribution of the supernova matter with fixed Y_p and possible effects on the supernova nucleosynthesis. We summarize our work in Sec. 5.

2 Relativistic Mean Field Approach

Supernova matter is composed of nucleons, electrons, neutrinos, their anti-particles and photons. Neutrinos are trapped at high density and are emitted from the so-called neutrino-sphere, where the neutrinos become free streaming. Inside ν-sphere, the dense matter is characterized by a fixed lepton fraction (lepton-to-baryon ratio) Y_L, due to the neutrino trapping. In this case, there are three conserved quantities; baryon number B, total charge C, and lepton number L. Then particle chemical potentials are represented by corresponding three chemical potentials,

$$\mu_i = B_i\mu_B + C_i\mu_C + L_i\mu_L \ , \tag{1}$$

where μ_B, μ_C, μ_L are baryon, charge and lepton chemical potentials, and B_i, C_i, L_i are baryon, charge and lepton numbers of particle species i, respectively.

In this section, we show the results of fixed Y_L. Outside of ν-sphere, the lepton fraction is no longer conserved. Instead, the electron fraction Y_e, is kept constant approximately. The density at the ν-sphere surface will be discussed in subsection 2.4.

2.1 RMF Lagrangian and parameter set

Relativistic Mean Field (RMF) approach has been developed as an effective theory to describe the nuclear matter saturation in a simple way [20]. Having improvements to include meson self-coupling terms, it describes well the binding energies of neutron-rich unstable nuclei in addition to nuclear matter and stable nuclei [21].

In this work, we adopt an RMF parameter set TM1 [21]. It has been demonstrated that this parameter set TM1 can reproduce nuclear properties including proton- and neutron-rich unstable nuclei. In addition, the EoS table with TM1 has been successfully applied to neutron stars and supernova explosions [17,26–28]. Therefore, it is expected to be reliable also in describing two-phase coexistence in supernova matter, which contains asymmetric nuclear matter having proton-to-neutron ratio varying in a wide range.

The Lagrangian contains three meson fields; scalar-isoscalar σ meson, vector-isoscalar ω meson, and vector-isovector ρ meson. In this work, we limit the constituent particles as nucleons, electrons, electron-neutrinos, their anti-particles and photons. The explicit form of the Lagrangian including leptons is given as follows.

$$
\begin{aligned}
\mathcal{L} =& \bar{\psi}_N \left(i\partial\!\!\!/ - M - g_\sigma \sigma - g_\omega \omega\!\!\!/ - g_\rho \tau^a \rho\!\!\!/^a \right) \psi_N \\
&+ \frac{1}{2}\partial^\mu \sigma \partial_\mu \sigma - \frac{1}{2} m_\sigma^2 \sigma^2 - \frac{1}{3} g_2 \sigma^3 - \frac{1}{4} g_3 \sigma^4 \\
&- \frac{1}{4} W^{\mu\nu} W_{\mu\nu} + \frac{1}{2} m_\omega^2 \omega^\mu \omega_\mu - \frac{1}{4} R^{a\mu\nu} R^a_{\mu\nu} + \frac{1}{2} m_\rho^2 \rho^{a\mu} \rho^a_\mu + \frac{1}{4} c_3 \left(\omega_\mu \omega^\mu \right)^2 \\
&+ \bar{\psi}_e \left(i\partial\!\!\!/ - m_e \right) \psi_e + \bar{\psi}_\nu i\partial\!\!\!/ \psi_\nu - \frac{1}{4} F_{\mu\nu} F^{\mu\nu} \ , \\
W_{\mu\nu} =& \partial_\mu \omega_\nu - \partial_\nu \omega_\mu \ , \\
R^a_{\mu\nu} =& \partial_\mu \rho^a_\nu - \partial_\nu \rho^a_\mu + g_\rho \epsilon^{abc} \rho^{b\mu} \rho^{c\nu} \ , \\
F_{\mu\nu} =& \partial_\mu A_\nu - \partial_\nu A_\mu \ .
\end{aligned} \tag{2}
$$

In this section, photon contributions to pressure, energy and entropies are included, but we have dropped the photon-couplings to charged particles (See Sec. 3 on this point).

In a mean field approximation, three meson fields are replaced to their expectation values. Self-consistency condition for these values can be derived in a standard manner, as $\partial P/\partial x = 0$ where x represents the meson field expectation value and P denotes the pressure. The chemical equilibrium conditions for given conserved densities ρ_k are expressed as $\partial P/\partial \mu_k = \rho_k$. We solve these conditions in a multi-dimensional Newton's method by iteration.

2.2 Two-phase coexistence treatment in RMF

We apply the mean field approximation to the liquid and gas phases separately. In this treatment, we implicitly assume that two coexisting (liquid, gas) phases are uniform and have infinite size. We solve chemical and thermal equilibrium conditions between the liquid and gas phases.

In order to make liquid and gas phases coexist at equilibrium, we must apply the Gibbs conditions rather than the Maxwell construction, since the number of conserved quantity (= 3) is larger than one. The Gibbs conditions are given as follows,

$$
(1-\alpha)\, \rho_k^{Liq.} + \alpha \rho_k^{Gas} = \rho_k \ , \quad \mu_k^{Liq.} = \mu_k^{Gas} \ , \quad P^{Liq.} = P^{Gas} \ , \tag{3}
$$

where $k = B, C, L$. The quantities labeled by $Liq.$ and Gas are those of liquid and gas phases, respectively. The gas volume fraction, α, is a number between zero and unity. We solve these conditions by using multi-dimensional Newton's method, in which the dimension is five in the asymmetric nuclear matter ($k = B, C$) and seven in the supernova matter ($k = B, C, L$), where the variables are $\rho_k^{Liq.}, \rho_k^{Gas}$ and α. See Appendix A for the numerical technique at very low densities.

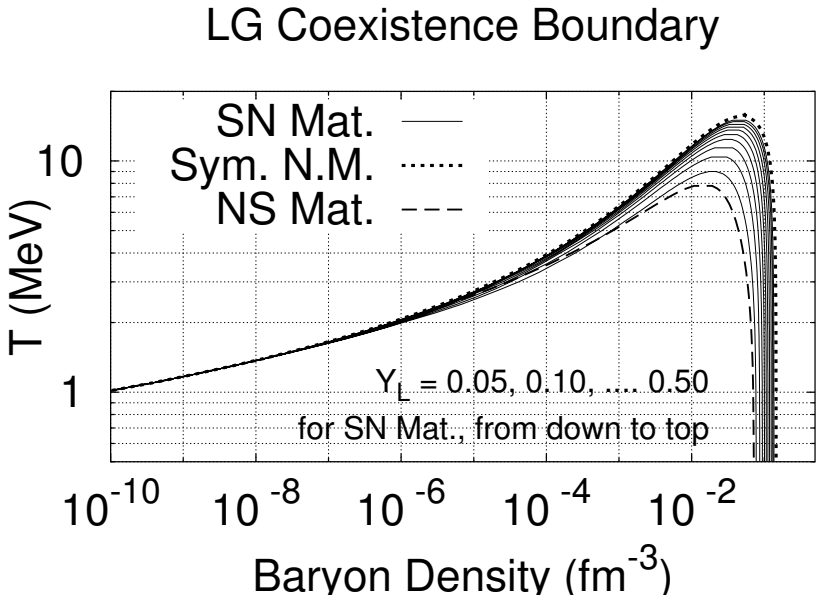

Fig. 1. Boundary of liquid-gas coexisting region in supernova matter (solid curves) in comparison with symmetric nuclear matter ($Y_p = 0.5$, dotted line) and neutrino-less supernova matter (or finite temperature neutron star matter, $\mu_L = 0$, dashed line).

We show the liquid-gas coexisting region of supernova matter in Fig. 1. See Appendix B for the procedure to determine this boundary. The solid curves show the boundary of coexisting region, and two phases coexist below the boundary. We find that the critical temperature is very high $T_c \sim$14 MeV for $Y_L = (0.3 - 0.4)$, which is the ratio expected in actual supernova explosions. These critical temperatures are much higher than those in neutrino-less supernova matter (dashed line) and comparable to those in the symmetric nuclear matter (dotted line). The boiling points of supernova matter remain to be $T_{boil} \sim 1$ MeV even at very low densities for all lepton fractions.

The large value of T_{boil} is due to symmetrization of nuclear matter by leptons. Since Y_L is kept constant but Y_p is not fixed, the supernova matter searches its minimum in free energy by changing Y_p. In high density supernova matter, the lepton fraction is shared by electrons and neutrinos ($2/3Y_L < Y_e < Y_L$), then the net neutrino fraction and the lepton chemical potential become positive ($\mu_L = \mu_\nu > 0$). Compared to neutrino-less supernova matter ($\mu_L = 0$), this positive μ_L in supernova matter helps to raise value of $Y_e (= Y_p)$ ($\mu_e = -\mu_C + \mu_L$), and to symmetrize nuclear matter. We have to remark that fixing Y_L is not appropriate at low density ($< 10^{-5}$ fm^{-3}) outside the ν-sphere. We will discuss on this point later. At very low baryon densities, electrons become non-degenerate, i.e. electron and anti-electron densities are much higher than the net electron densities because of small electron mass, and this also applies to neutrinos. Hence, electron and neutrino chemical potentials become small, and the charge chemical potential also becomes small.

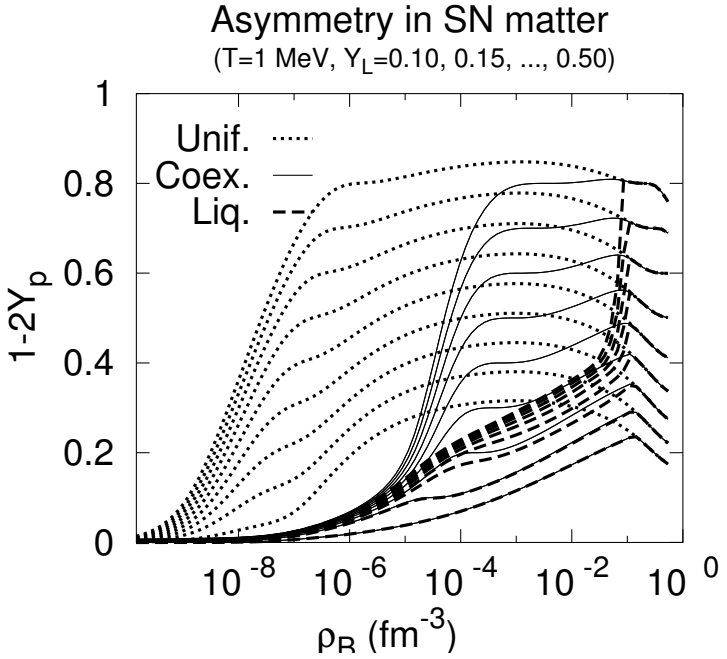

Fig. 2. Asymmetry parameter $\delta = 1 - 2Y_p$, of supernova matter as a function of baryon density at $T = 1$ MeV. Dotted, solid and dashed curves show the asymmetry parameter in uniform (homogeneous), two-phase coexisting, and the liquid part of coexisting matter, respectively.

This causes nuclear matter symmetric.

In order to demonstrate this point, we show the density dependence of the asymmetry parameter of supernova matter in Fig. 2. Dotted, solid and dashed curves show the asymmetry parameter $\delta = 1-2Y_p$ in uniform (homogeneous), two-phase coexisting, and the liquid part of coexisting matter, respectively. It is clear that, as the baryon density decreases, asymmetry parameter decreases and this tendency is stronger in the coexisting region. In uniform matter, the asymmetry decreases rapidly at around $\rho_B < 10^{-7}$ fm^{-3}, where leptons dominate pressure and energy density, as shown later in Fig. 4. This is consistent with the above consideration on the lepton dominance. On the other hand, the asymmetry parameter start to decrease at much higher density in coexisting matter. This symmetrization is mainly due to the symmetry energy in nuclear matter. Since the baryon density in the liquid part of matter is around ρ_0, nucleons can gain symmetry energy by reducing the asymmetry. As shown by dashed lines, the asymmetry decreases quickly in the liquid part in the coexisting region.

We turn our attention to one of the characteristic features of the liquid-gas coexisting region in supernova matter, which allows many fragments to be formed even at very low densities. First we define a new quantity, gas fraction Y_g, Y_g = (baryons in gas phase)/(total baryons) $\equiv \alpha\rho_B^{Gas}/\rho_B$ as a

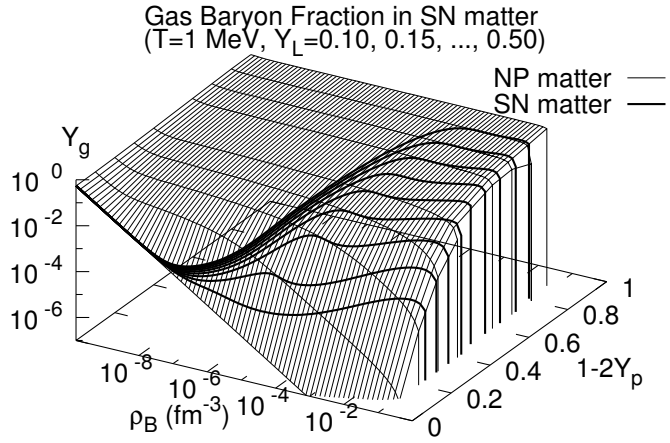

Fig. 3. Gas fraction Y_g in asymmetric nuclear matter (thin line surface) and in supernova matter (thick lines) as a function of the baryon density and the asymmetry, $\delta = 1 - 2Y_p$, at $T = 1$ MeV.

measure of bulk fragment yield. For a rough estimate, we can adopt the normal nuclear matter density ρ_0 for the baryon densities in the liquid phase. After we substitute these baryon densities ρ_0 and ρ_B^{Gas} for the Gibbs condition, we can obtain the following relation,

$$\alpha \simeq \frac{\rho_0 - \rho_B}{\rho_0 - \rho_B^{Gas}} \ . \tag{4}$$

For example, all baryons are bound in nuclei at $Y_g = 0$. Smaller Y_g means larger amount of fragments. In Fig. 3, we show the gas fraction in nuclear matter composed of neutrons and protons (np matter) and supernova matter as a function of the baryon density and the asymmetry parameter, calculated in the RMF model. We fix Y_p for calculations of np matter. The behavior of Y_g in np matter is smooth. In symmetric nuclear matter ($Y_p = 0.5$), both of the liquid and gas phases are symmetric, and the density in each phase is constant in the coexisting region. Then the gas fraction can be expressed by liquid, gas and the given average densities ($\rho_B^{Liq.} \simeq \rho_0, \rho_B^{Gas}, \rho_B$) as

$$Y_g \simeq \frac{\rho_B^{Gas}(\rho_0 - \rho_B)}{\rho_B(\rho_0 - \rho_B^{Gas})} \ . \tag{5}$$

This is a monotonically decreasing function of the baryon density and very small in the density range under consideration ($\rho_B^{Gas} \ll \rho_B < \rho_0$). When the asymmetry increases, the liquid phase loses the symmetry energy and nucleons are emitted to the gas phase, while Y_g is still a decreasing function of ρ_B.

The behavior of Y_g in supernova matter is very different from that in np

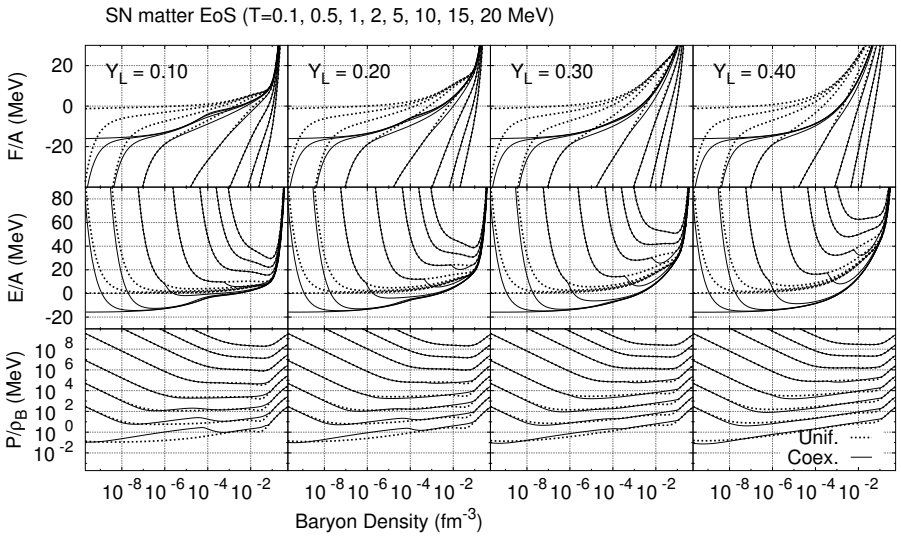

Fig. 4. Equation of state of supernova matter for lepton fractions $Y_L = 0.1$, 0.2, 0.3 and 0.4. Temperatures are T =0.1, 0.5, 1, 2, 5, 10, 15 and 20 MeV, from top to down (from down to top) for F/A (E/A and P/ρ_B). Results for uniform supernova matter are shown by dotted curves, and those with liquid-gas coexistence are shown by solid curves. For energies per baryon (E/A) and free energies per baryon (F/A), nucleon mass is subtracted. The pressures are increased by a factor of 10 from low to high temperatures (from bottom to top) for clarity of plot.

matter. As shown by the thick lines in Fig. 3, Y_g first decreases then grows again as the baryon density decreases. This behavior is determined by the proton fraction Y_p. In the medium density region ($\rho_B = (10^{-7} - 10^{-2})$ fm^{-3}), matter becomes symmetric as ρ_B decreases, and the gas baryon fraction decreases to the symmetric nuclear matter value in Eq. (5). Therefore, baryons favor liquid state than nucleon gas in the coexisting region. After reaching symmetric matter, gas fraction increases again according to Eq. (5). It is also interesting to note that the proton fraction Y_p of supernova matter shows clear Y_L dependence at $\rho_B > 10^{-5}$ fm^{-3}, while Y_p is almost independent on Y_L at $\rho_B < 10^{-5}$ fm^{-3}. This density roughly corresponds to the neutrino-sphere, inside which neutrinos are trapped in supernova core.

2.3 Supernova Matter Equation of State

We show the EoS of supernova matter with (without) two-phase coexistence by solid (dotted) lines in Fig. 4. In both of the cases, energy and pressure increase at high densities above ρ_0 because of the vector meson contributions. At very low densities, lepton contributions become dominant, because lepton pressure and energy densities are finite even with $\rho_B = 0$ at finite temper-

atures. In uniform matter, the nuclear pressure and energy become close to free-gas values $P_N/\rho_B \to T, E_N/A \to 3T/2$. Between these two extremes of density, we can find the effects of two-phase coexistence.

In two-phase coexistence, binding energy is gained by making liquid phase whose baryon density is around ρ_0. At low temperatures, since nuclear matter tends to be symmetric and liquid phase is dominant in a wide range of densities, liquid part of energy per baryon approaches toward -16 MeV.

At large lepton fractions ($Y_L = 0.3 - 0.4$), the pressure behaves as in the case of Maxwell construction for volume instability; pressures in the coexisting region are lower (higher) at low (high) densities than in uniform matter during the coexistence. On the other hand, we can find double phase transition behavior in lepton deficient matter ($Y_L = 0.1 - 0.2$); while the pressure behaves as in the case of volume instability at higher densities ($\rho_B \geq 10^{-4}$ fm^{-3}), there is another overtaking in the density region of $\rho_B = 10^{-8} \sim 10^{-4}$ fm^{-3}. At these densities, the matter becomes unstable to the small fluctuations of proton fraction, and liquid part of the matter becomes rapidly symmetric as the density decreases. Thus the overtaking of the pressure in the low-density region may be suggesting the phase transition in the isospin degrees of freedom.

2.4 Adiabatic Paths

After the core bounce, some part of supernova matter becomes so dense as to trap neutrinos, and it expands almost adiabatically because of constant Y_L. High entropy ($S/B \geq 10$) part of the matter inside of the ν-sphere would be later ejected to outside [24]. Therefore, it is important to examine supernova matter along the adiabatic paths. In Fig. 5, we show the adiabatic paths in supernova matter with fixed lepton fractions of $Y_L = 0.1 \sim 0.5$. Entropy per baryon is taken to be $S/B = 1 \sim 100$. At very high entropies such as $S/B = 100$, adiabatic paths are almost independent on Y_L because of the lepton dominance. At lower entropies, we can clearly see nuclear and coexistence effects. While adiabatic paths in uniform matter (dashed lines) evolve very smoothly, those with two-phase coexistence (thin solid lines) bend closer to the boundary of coexisting region. This bending comes from the latent heat and suggests that significant amount of nuclei are formed around the boundary.

The assumption of constant Y_L breaks down outside of the ν-sphere. Although it is necessary to determine the position of ν-sphere by neutrino-transport calculation for precise estimate, we here consider the trapping density ρ_{trap} at which $\mu_L = \mu_\nu = T$ as an approximate density at the ν-sphere. This condition always provides lower limit of the ν-trapping density $\mu_L \geq$

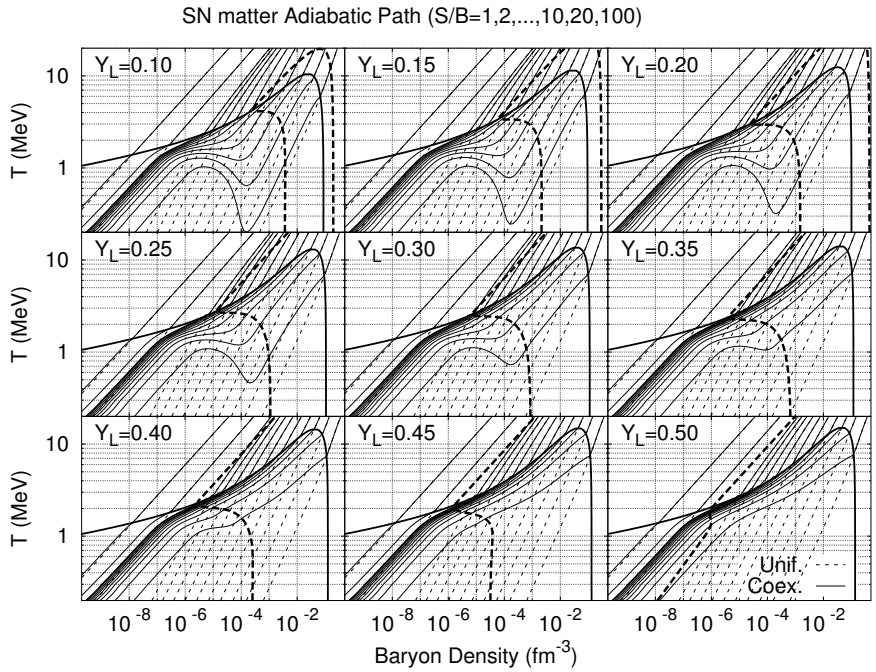

Fig. 5. Adiabatic paths in supernova matter calculated in RMF. Thin solid (dashed) lines show adiabatic paths of supernova matter with (without) the liquid-gas coexistence. Thick solid lines are the boundary of coexisting region. Thick dashed lines denote the contour of $\mu_L = T$. Each adiabat corresponds to entropy per baryon $S/B = 1, 2, ..., 10, 20, 100$. The panels are in the case of lepton fraction $Y_L = 0.1$, 0.15, ..., 0.5 from upper-left to lower-right, respectively.

0 [15,16]. Thick dashed lines in Fig. 5 show these densities. The trapping density ρ_{trap} strongly depends on the lepton fraction, and it is consistent with the well-known value, $10^{-4} \sim 4 \times 10^{-5}$ fm^{-3}, at realistic lepton fractions $Y_L = (0.3 - 0.4)$.

In the coexisting region, the electron fraction Y_e increases due to the symmetrization of liquid, then the neutrino fraction is suppressed. As a result, the trapping density is shifted to higher direction. We come back the point later in Sec.4.

3 Fragment Distribution in Supernova Matter

Observations in the previous section tell us that it would be possible for supernova matter to experience the liquid-gas phase transition before it is ejected to outside. Therefore, it is interesting to study the composition of ejecta experienced the phase coexistence. However, we have assumed that the

coexisting two phases are infinite. It is also to be noted that nuclear matter in the liquid phase is more symmetric than in the gas phase. As a result, the Coulomb energy is expected to be large, which we have neglected in the previous section, and the infinite matter in the liquid phase will fragment into finite nuclei. Although the effects of these nuclear formation on EoS may not be very large [16], the broad fragment distribution would affect the later evolution of expanding matter such as electron capture and seed formation for the r-process. Therefore, in this section, we evaluate the fragment yield in a fragment-based statistical model.

3.1 Statistical Model of Fragments

In order to describe distribution of finite nuclei, we utilize a fragment-based statistical model. This kind of statistical models have been widely used in heavy-ion collision studies [4–7] as well as in astrophysics, as referred to the nuclear statistical equilibrium (NSE) [11,29]. In NSE, we solve the statistical equilibrium condition among nucleons, fragments, leptons and photons in fragment-based grand canonical ensemble. In this work, we have ignored relativistic corrections and anti-particle contributions of fragments, and fragments are assumed to follow the Boltzmann statistics, while leptons are treated relativistically. The ensemble averages can be generated from the grand potential,

$$\Omega = -PV = -VT\sum_i \rho_f - P_\ell V - P_\gamma V \ , \tag{6}$$

$$\rho_f = \zeta_f(T)\left(\frac{M_f T}{2\pi\hbar^2}\right)^{3/2}\exp\left(\frac{B_f+\mu_f}{T}\right) \ , \tag{7}$$

$$\mu_f = Z_f(\mu_p - m_N) + N_f(\mu_n - m_N) \ , \tag{8}$$

where ρ_f, M_f, B_f and μ_f denote the density, mass, binding energy and the chemical potential of fragment f, and P_ℓ and P_γ are the lepton and photon pressures, respectively. The intrinsic partition function, $\zeta_f(T)$, has been calculated by using the level density formula for fragments with $A_f \geq 5$ [6],

$$\begin{aligned}\zeta_f(T) &= \sum_i g_f^{(i)}\exp\left(-E_f^{*(i)}/T\right) \\ &\simeq g_f^{(g.s.)} + \frac{c_1}{A_f^{5/3}}\int_0^\infty dE^* e^{-E^*/T}\ \exp(2\sqrt{a_f E^*}) \ , \\ a_f &= \frac{A_f}{8}\left(1 - c_2 A_f^{-1/3}\right)\ (\mathrm{MeV}^{-1}) \ , \quad c_1 = 0.2\ (\mathrm{MeV}^{-1}) \ , \quad c_2 = 0.8 \ ,\end{aligned} \tag{9}$$

where $g_f^{(i)} = 2j_f^{(i)} + 1$ is the spin degeneracy of the energy level at excitation energy $E_f^{*(i)}$ of the fragment species f.

In NSE, the nuclear binding energy B_f plays an essential role. Fragment yields are sensitive to the binding energy modification due to, for example, the medium effects in supernova matter. In studies of heavy-ion collisions, since the density and its fluctuation are large, the repulsive interfragment Coulomb potentials are taken into account explicitly rather than in the form of mass modification. In supernova matter under consideration, attractive electron-fragment Coulomb potential effects are more important. Since electron density is not negligible and almost constant, we ignore inter-fragment Coulomb potentials and the electron effects on intrinsic fragment Coulomb energies are incorporated in the form of binding energy modification. We have used the Wigner-Seitz approximation in evaluating the Coulomb energy correction [16] to the binding energy of nuclei adopted in NSE. We assume that the electrons are distributed uniformly in a sphere with radius R_{ef} which is determined to cancel the charge of the fragment f at a given electron density ρ_e.

$$B_f(\rho_e) = B_f(0) - \Delta V_f^{Coul}(\rho_e) \ , \tag{10}$$

$$\Delta V_f^{Coul} = -\frac{3}{5}\frac{Z_f^2 e^2}{R_0}\left(\frac{3}{2}\,\eta_f - \frac{1}{2}\,\eta_f^3\right) \ , \quad \eta_f \equiv \frac{R_{0f}}{R_{ef}} = \left(\frac{\rho_e}{Z_f\rho_0/A_f}\right)^{1/3} \ , \tag{11}$$

where $B_f(0)$ is the nuclear binding energy in vacuum, and R_{0f} is the nuclear radius.

It is important to note that the Coulomb energy correction, $\Delta V_f^{Coul}(\rho_e)$, contains the term proportional to $\rho_e^{1/3}$. Because of this functional form, the correction is meaningfully large even at $\rho_B = 10^{-6}\rho_0$. For example, when the electron fraction is $Y_e = 0.3$, the reduction of the Coulomb energy for heavy nuclei amounts to 90 % of the total Coulomb energy at $\rho_B = \rho_0$, and the reduction is around 10 MeV even at $10^{-6}\rho_0$. The increase of binding energy acts to enhance heavy nuclei, and some nuclei beyond the dripline at vacuum or unstable against fission, can be stabilized in supernova matter. Finite gas nucleon density also plays a role to form nuclei beyond the dripline tentatively by the balance of nucleon absorption and emission. We have adopted the mass table of Myers and Swiatecki [30], which is based on the Thomas-Fermi model with shell correction for about 9000 kinds of nuclei.

Since nuclear binding energies depend on the electron density, we have to solve the chemical equilibrium condition of nuclei and leptons in supernova matter in a consistent way to satisfy $F_\mu = \mu_p + \mu_e - \mu_n - \mu_\nu = 0$. Provided that the baryon density and temperature are given, and that the charge and lepton densities are fixed as $(\rho_C, \rho_L) = (0, Y_L\rho_B)$, all the particle densities are determined if the average proton fraction (Y_p) is given,

$$(1-Y_p)\,\rho_B = \sum_f N_f \rho_f(\mu_n,\mu_p,B_f(\rho_e)) \equiv \overline{\rho}_n(\mu_n,\mu_p,\rho_e)\ , \tag{12a}$$

$$Y_p\,\rho_B = \sum_f Z_f \rho_f(\mu_n,\mu_p,B_f(\rho_e)) \equiv \overline{\rho}_p(\mu_n,\mu_p,\rho_e)\ , \tag{12b}$$

$$Y_p\,\rho_B = \rho_e(\mu_e)\ , \quad (Y_L - Y_p)\,\rho_B = \rho_\nu(\mu_\nu)\ , \tag{12c}$$

where $\overline{\rho}_n$ and $\overline{\rho}_p$ are the neutron and proton densities including those in nuclei. We can easily solve last two conditions in Eqs. (12c) numerically, and derivatives of μ_e and μ_ν with respect to Y_p can be obtained as $d\mu_e/dY_p = \rho_B\,(d\rho_e/d\mu_e)^{-1}$ and $d\mu_\nu/dY_p = -\rho_B\,(d\rho_\nu/d\mu_\nu)^{-1}$. Once Y_p is given, first two equations are the same as usual conditions in fragment-based statistical models. By using the charge neutrality condition $\rho_e = Y_p\rho_B$, we can get the derivatives of μ_n and μ_p with respect to Y_p as,

$$\begin{pmatrix} \partial\overline{\rho}_n/\partial\mu_n\ ,\ \partial\overline{\rho}_n/\partial\mu_p \\ \partial\overline{\rho}_p/\partial\mu_n\ ,\ \partial\overline{\rho}_p/\partial\mu_p \end{pmatrix} \begin{pmatrix} d\mu_n \\ d\mu_p \end{pmatrix} = \rho_B\ dY_p \begin{pmatrix} -1-\partial\overline{\rho}_n/\partial\rho_e \\ 1-\partial\overline{\rho}_p/\partial\rho_e \end{pmatrix}\ . \tag{13}$$

Therefore, we can solve the chemical equilibrium condition, $F_\mu = 0$, by the Newton's method, $\delta F_\mu = -F_\mu/\left(dF_\mu\left(Y_p\right)/dY_p\right)$.

3.2 Gas Fraction and Equation of State in a Statistical Model

Compared to RMF, there is no sharp phase transition in NSE because of the finite size of fragments. Although we can see kink-like behavior in the nuclear part of energy per baryon as a function of the temperature (caloric curve), this kink is not clear enough to define the boiling point as seen in Fig. 6. There are several definitions of T_{boil} proposed in the literature. For example, T_{boil} is proposed to be well defined at the peak of M_2/M_1 by Bauer [7]. The n-th moment of light fragments, M_n, is defined as $M_n \equiv \sum_f A_f^n \rho_f$. Another way is to define T_{boil} by the peak of the light fragment mass variance-to-average ratio, $\xi \equiv \sigma^2(A_f)/ < A_f >$, which becomes small when one fragment (or nucleon) dominates, and becomes unity when the mass distribution is a Poissonian. We show these ratios in the upper-left panel of Fig. 6. At high densities, these definitions give reasonable boiling points, but at low densities, the peak of M_2/M_1 becomes dull, and ξ shows two peaks. From fragment distributions, we find that the two peak structure appears due to the formation of α which can be comparable to neutrons at very low densities, where gas part becomes almost symmetric. In Fig. 7, we show the temperatures at local maxima of ξ by dot-dashed lines. This formation of α makes also M_2/M_1 peak dull. Therefore, we here define the boiling point as the peak of the light fragment mass variance-to-average ratio ξ', where we exclude α particle in the calculation of the light fragment mass average and variance. As shown in the

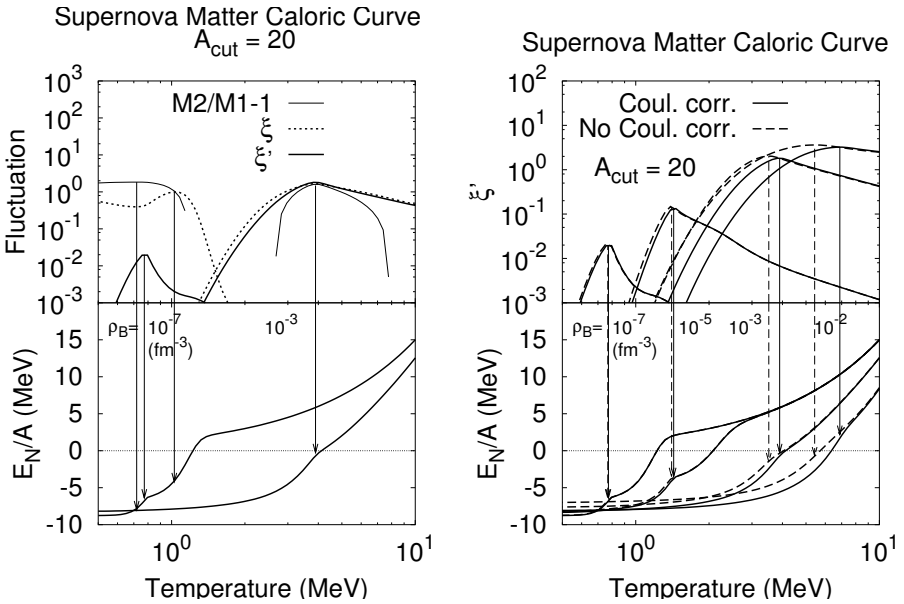

Fig. 6. Left: Mass moment ratio (upper panel) and caloric curve (lower) of supernova matter with $Y_L = 0.35$ at $\rho_B = 10^{-7}$ and 10^{-3} fm^{-3}. In the upper panel, mass moment ratios, M_2/M_1 (thin solid lines), $\xi = \sigma^2(A_f)/ < A_f >$ (with α, dotted lines), ξ' (same as ξ but without α, thick solid lines) are shown. Right: ξ' (upper panel) and caloric curve (lower) of supernova matter with $Y_L = 0.35$ at baryon densities $\rho_B = 10^{-7}, 10^{-5}, 10^{-3}$ and 10^{-2} fm^{-3}. Results with Coulomb correction (solid lines) and without Coulomb correction (dashed lines) are compared.

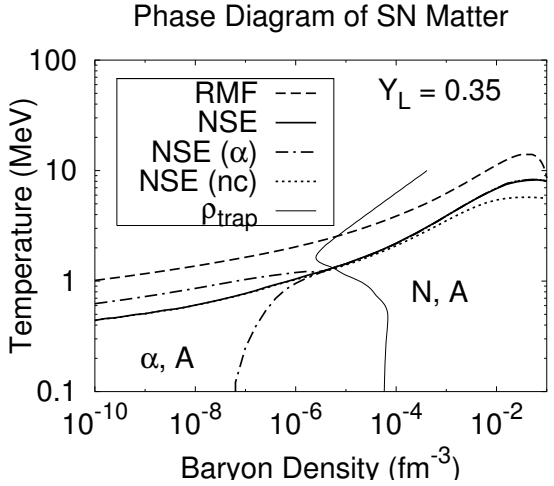

Fig. 7. Liquid-gas coexisting region of supernova matter with $Y_L = 0.35$ calculated in NSE (thick solid line) in comparison with RMF results (dashed line). Results without Coulomb correction is shown by dotted curve. The thin solid line shows the trapping density where $\mu_L = T$. Boiling point in the statistical model has been determined as the maximum point of mass variance-to-average ratio without $\alpha(\xi')$, while there appear two local maxima when we include the contribution of α particle, as shown by dot-dashed curves.

Table 1
Boiling points in NSE at $Y_L = 0.35$ as a function of the baryon density. Results with (NSE) and without (NSE, nc) Coulomb corrections are shown.

ρ_B(fm^{-3})	10^{-10}	10^{-9}	10^{-8}	10^{-7}	10^{-6}
T_{boil}(NSE) (MeV)	0.46	0.51	0.61	0.77	1.04
T_{boil}(NSE,nc) (MeV)	0.45	0.50	0.61	0.76	1.03
ρ_B(fm^{-3})	10^{-5}	10^{-4}	10^{-3}	10^{-2}	10^{-1}
T_{boil}(NSE) (MeV)	1.44	2.20	3.89	6.89	8.06
T_{boil}(NSE,nc) (MeV)	1.39	2.09	3.51	5.43	5.61

solid lines in Fig. 6, the peak position of ξ' is well defined at any density. In addition, this boiling point corresponds to the kink position in the caloric curve.

In Fig. 7, we show the density dependence of T_{boil} with fixed $Y_L = 0.35$, in comparison with the RMF results. This condition of fixed Y_L will be relevant at higher density than the density at the ν-degenerate plotted with thick short dashed line. We find that the boiling points in NSE are lower than those in the two phase treatment of the RMF model by about a factor of two. The reduction of T_{boil} is a natural consequence of finite size of nuclei. Because the intrinsic Coulomb energy cannot be completely removed by electrons at densities $\rho_B < \rho_0$, nuclei are limited to have finite size. Then nuclei loses surface energy in addition to the Coulomb energy, and gas nucleons are favored. However, it is worthwhile to note that the qualitative behavior of T_{boil} is similar to that in RMF, and they are still high enough, $T_{boil} \geq 0.5$ MeV for $\rho_B > 10^{-9}$ fm^{-3}. We tabulate the boiling points at $\rho_B = 10^{-10} \sim 10^{-1}$ fm^{-3} in Table 1.

In the RMF treatment, one of the most characteristic features in the coexisting region is the reduction of the gas fraction. This also applies to the NSE results. We have defined the gas fraction as the ratio of free (isolated) nucleon density to the total baryon density, $Y_g \equiv (\rho_p + \rho_n)/\rho_B$. As shown in Fig. 8, gas fraction behaves similarly to that in RMF results; as the baryon density decreases, it quickly becomes very small until $\rho_B \sim 10^{-8}$ fm^{-3}, and gradually grows at lower densities again. In addition, it is interesting to note that Y_g curves within the statistical model have the second minimum at $\rho_B \sim 10^{-3}$ fm^{-3}. Supernova matter favors nuclear fragment (nucleus) state rather than nucleon gas at these densities. We call these minimum regions as the first ($\rho_B \sim 10^{-7}$ fm^{-3}) and the second ($\rho_B \sim 10^{-3}$ fm^{-3}) fragment windows, respectively. The first one is caused by the drastic isospin-symmetrization of supernova matter by leptons at low baryon densities. The second fragment window is specific to NSE. The mechanism of this appearance is not very clear, but we find that these two minima converges to one when we use the liquid drop mass formula for the nuclear binding energies and ignore the sur-

face term.

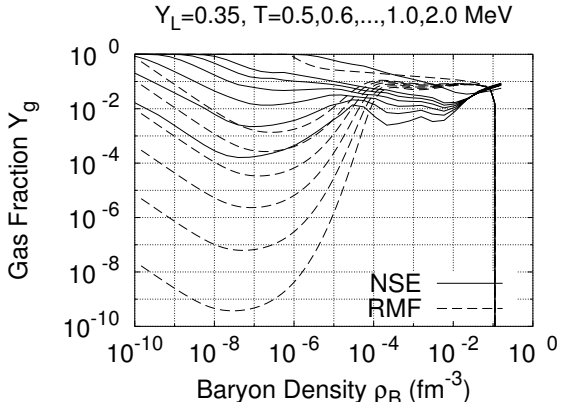

Fig. 8. Gas fraction in supernova matter as a function of the baryon density at $Y_L = 0.35$. Results in NSE (RMF) are shown by solid (dashed) lines. Temperatures are taken to be $T = 0.5, 0.6, ..., 1.0$ and 2.0 MeV from bottom to top.

In Fig. 9, we show the EoS in NSE at $T = 5$ and 1 MeV with $Y_L = 0.35$, in comparison with those in RMF with the Thomas-Fermi approximation for a dominant configuration [17] (RMF+TF, dotted lines), RMF with two-phase coexistence (RMF(coex.), dashed lines), and homogeneous RMF (RMF(unif.), dot-dashed lines). We find that the finiteness of nuclei does not affect the EoS at high densities, $\rho_B \geq 10^{-2}$ fm^{-3} (10^{-4} fm^{-3}) for $T = 5$ MeV (1 MeV), but modifies the density dependence of the pressure at lower densities, as seen in the difference between RMF(coex.) and RMF+TF. Compared with the EoS in RMF+TF, the present NSE results give very similar pressures, except for the density region $\rho_B \sim 10^{-3}$ fm^{-3}(10^{-6} fm^{-3}) for $T = 5$ MeV (1 MeV), where the pressure are different by $10 \sim 20$ %. These densities correspond to the region where the given temperatures are close to the boiling points.

The agreement of EoS in NSE and RMF+TF is somewhat surprising. There are three large differences in NSE and RMF+TF: (1) Nuclear masses are taken from the table [30] in NSE, while masses are calculated in RMF+TF. (2) Nucleon-fragment nuclear interactions are neglected in NSE, while they are included in RMF+TF. (3) One configuration is assumed in RMF+TF, while statistical ensemble is considered in NSE. Thus the above agreement might suggest that once nuclear masses are properly included, nuclear interactions between gas nucleon and fragments play a minor role in EoS.

3.3 Fragment Distribution and Coulomb Correction Effects

In this subsection, we investigate fragment distribution in the density range $10^{-5} \geq \rho_B \geq 10^{-2}$ fm^{-3}, starting from the trapping density to the density close to the critical point. We are most interested in the boundary of coexisting

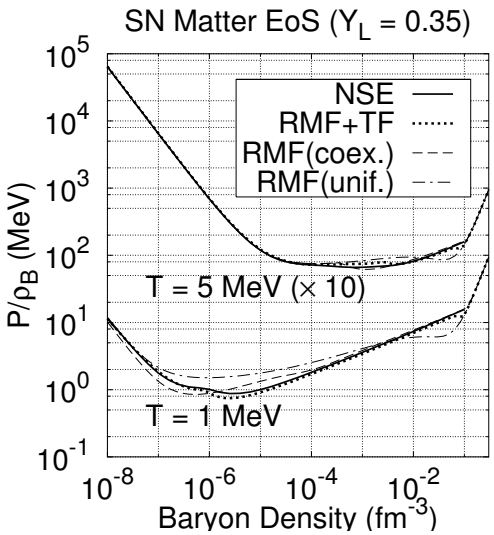

Fig. 9. Equation of state of the supernova matter in NSE in comparison with those in RMF models at $T = 1$ MeV (lower curves) and $T = 5$ MeV (upper curves, scaled up by a factor of 10). The solid, dotted, dashed and dot-dashed line denote EoS in NSE, RMF with Thomas-Fermi approximation model (RMF+TF) [17], the liquid-gas coexisting RMF model (RMF(Coex.)) and homogeneous RMF model (RMF(Unif.)), respectively.

region at the temperatures around $T_{boil}(\rho_B)$. If the density is not very small, the freeze-out temperature T_{fo} is expected to be around or just below the boiling point T_{boil}. Below the boiling points, fragments are formed abundantly by absorbing many of gas nucleons, and nuclear *number* density of particles (sum of nucleon and fragment densities) becomes quickly smaller, then the mean free path for each particle becomes much longer. This rapid fragment formation makes the typical interaction intervals longer, and is expected to help the system to freeze-out. The condition of freeze-out should be studied more carefully.

We can see common features of the temperature dependence of fragment mass distributions in each row of Fig. 10. When the temperature is higher than the boiling point, the fragments almost obey the exponential distribution. At the temperature near the boiling point, the distribution shows the power-law like behavior up to some mass. A similar trend, $Y(A_f) \sim A_f^{-\tau}$, also appears in nuclear multifragmentation [1], where Y and A_f denote the fragment yield and mass. This power law was suggested by Fisher [2] for a mass distribution of droplets at around the critical point. As the temperature becomes lower than the boiling point, the distribution at each density becomes sharp around some mass number. The localization is caused by the small entropy and shell effects.

We show the results at $\rho_B = 10^{-5}$ fm^{-3} in Fig. 10 (first column), which corresponds to the density around the neutrino sphere. Most stable nuclei at

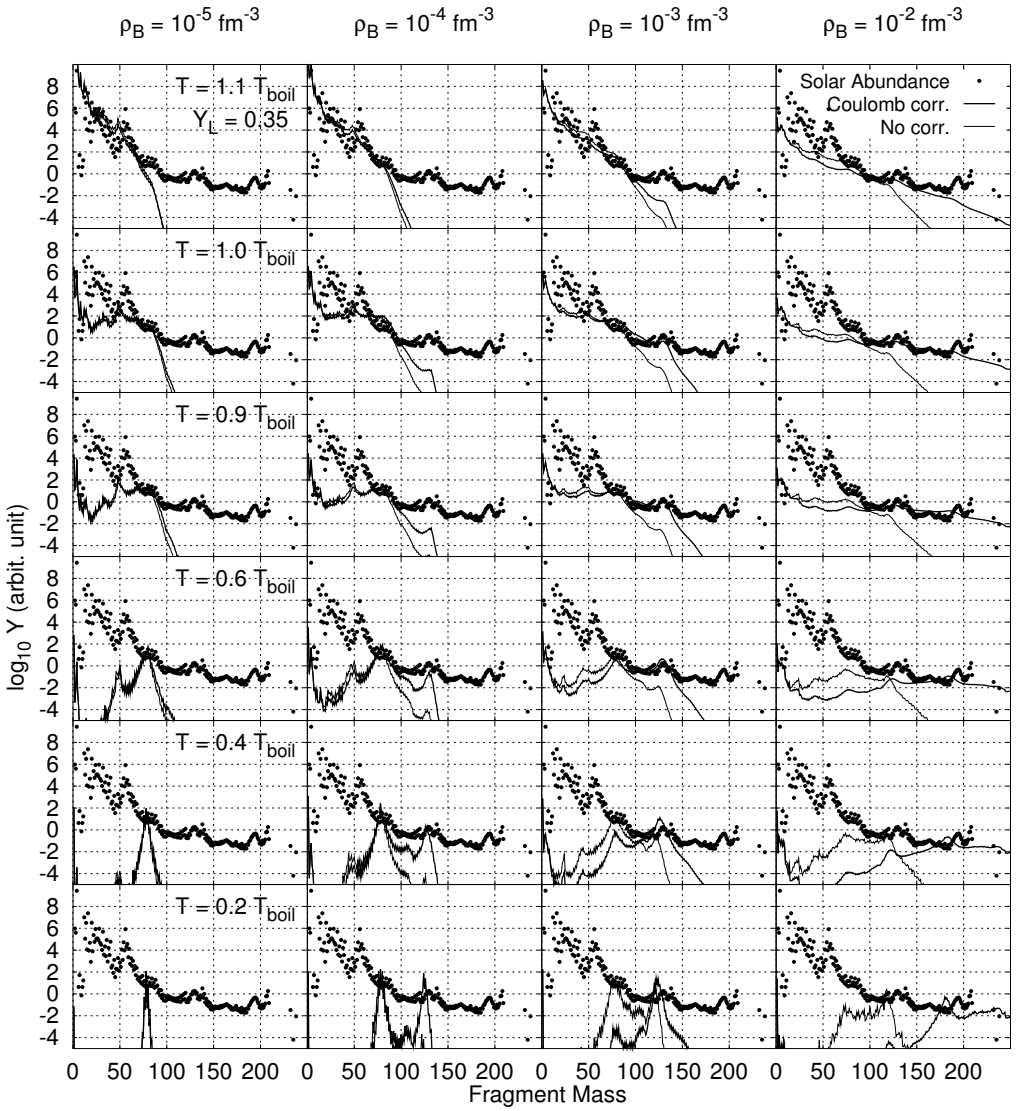

Fig. 10. The fragment distribution at $\rho_B = 10^{-5}$ fm^{-3} (first column), 10^{-4} fm^{-3} (second column), 10^{-3} fm^{-3} (third column), and 10^{-2} fm^{-3} (fourth column) with lepton fraction $Y_L = 0.35$ in comparison with the observed solar abundance (dots). Temperatures are taken to be $T = 0.2\ T_{boil} \sim 1.1\ T_{boil}$, where T_{boil} is the boiling point at each density. Thick and thin lines denote the distribution with and without Coulomb correction, respectively.

this density are those at around the first peak of r-process, as can be seen in the distribution at low temperatures. As a result, these nuclei are formed easily also at around the boiling point ($T = T_{boil} = 1.44$ MeV), in addition to nucleons, α, and $A \sim 50$ nuclei. The Coulomb correction effect is not large. At temperatures $T > 0.6\ T_{boil}$, the condition $\mu_L > T$ is satisfied as seen in Fig. 7.

Inside the ν-sphere, the Coulomb energy correction becomes significant. The second column in Fig. 10 shows the results at $\rho_B = 10^{-4}$ fm^{-3}. The

main component of the distribution shifts from the $A \sim 50$ nuclei at high temperatures to the first and second peaks of the r-process as the temperature goes down, although the behavior at higher temperatures seems to be almost the same at that of $\rho_B = 10^{-5}$ fm^{-3}. At $\rho_B = 10^{-3}$ fm^{-3}, power-law like behavior can be seen at around $T_{boil} = 3.89$ MeV up to the second peak of the r-process, as shown in the third column of Fig. 10. The center of the distribution shifts from the first peak of r-process without Coulomb correction to the second peak of r-process with Coulomb correction. The distribution at $\rho_B = 10^{-2}$ fm^{-3} (fouth column of Fig. 10) shows the same trend. It is interesting to find that the peak position in the NSE results is shifted downwards compared to the observed third peak of r-process. This shift mainly comes from the proton fraction of formed nuclei. The observed third peak of r-process is a consequence of the neutron magic number $N = 126$ and the Y_p along the r-process path. In the present NSE model calculation, having a smaller Y_p, nuclei beyond the neutron dripline appear easily at equilibrium.

We also give an example of isotope distribution at $Y_L = 0.35$ in Fig. 11. Here, we choose the boiling point, $T_{fo} = T_{boil}$, for the freeze-out temperature, as discussed at the beginning of this subsection. The upper-left, upper-right, lower-left and lower-right panels of Fig. 11 show the isotope distributions at $\rho_B = 10^{-2}, 10^{-3}, 10^{-4}$ and 10^{-5} fm^{-3}, respectively. At $\rho_B = 10^{-2}$ fm^{-3}, while the observed isotope ratio are well explained in the calculation from $Z = 20$ (Ca) to $Z = 92$ (U) with one overall normalization factor, much more neutron rich nuclei appear at equilibrium. For isotones with $N = 126$, nuclei with $Z = 54$ to $Z = 92$ are formed. This small Y_p in fragments, which comes from the large deviation from symmetric nuclear matter of the liquid phase at high densities as shown in Fig. 2, gives smaller mass number with $N = 126$. At lower densities, similar trends can be seen in the mass number range produced at around T_{boil}.

4 Fragment Distribution Outside of Neutrino-Sphere and Its Relation to Nucleosynthesis in Supernovae

In the previous section, we have discussed the fragment distribution in supernova matter around its boiling point at a given lepton fraction Y_L under charge and β equilibrium. With a decrease in density, the lepton chemical potential goes down to be smaller than T, and the neutrino degeneracy becomes weak. In addition, the mean free path of neutrinos becomes long. Then neutrinos start to move independently from baryons outside the ν-sphere.

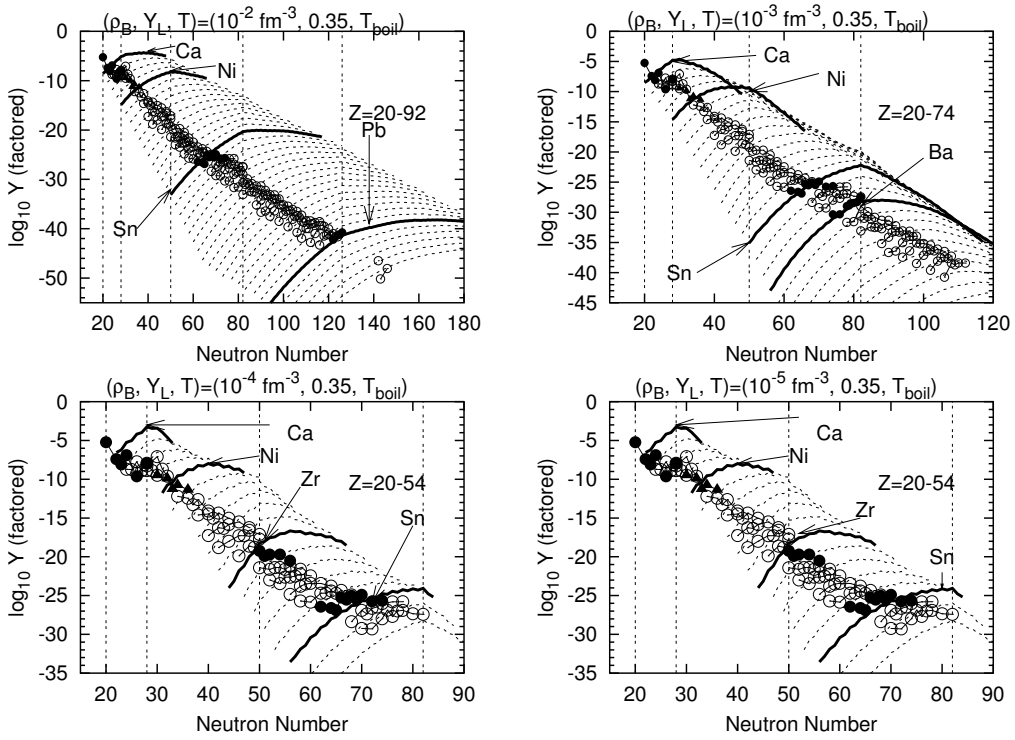

Fig. 11. Calculated even Z isotope distribution of supernova matter at $\rho_B = 10^{-2}, 10^{-3}, 10^{-4}$ and 10^{-5} fm^{-3} and $(T, Y_L) = (T_{boil}, 0.35)$ in comparison with the solar abundance by circle and triangle symbols. The boiling points are those for given densities. Yields are shifted, for clarify of plot, by a factor of 10 from $Z = 20$ (Ca) to larger Z nuclei (from top to bottom). One overall factor is chosen to get good global fit.

4.1 Fragment Formation Outside ν-sphere

Outside the ν-sphere, the β-equilibrium is not maintained, and number of protons, neutrons and electrons are separately conserved approximately, provided that the weak decay of neutrons and nuclei are slow enough compared to the dynamical expansion time scale. Under this condition, a constant value of $Y_p (= Y_e)$ is characteristic of the evolution of supernova matter outside the ν-sphere. The initial proton fraction Y_p outside the ν-sphere is determined in the preceding evolution of supernova matter specified by $(Y_L, S/B)$. Since fragment distribution is sensitive to Y_p, we can expect significant dependence on Y_L and S/B on the preceding path inside the ν-sphere. This is contrary to the situation that the nuclear matter is symmetrized and similar fragment distributions appear at very low densities for any fixed Y_L values under β-equilibrium.

There are three points to be discussed based on the equilibrium fragment statistical model. The first one is the Y_p value in Y_L fixed supernova matter at the ν-sphere, which approximately gives the proton fraction in the later

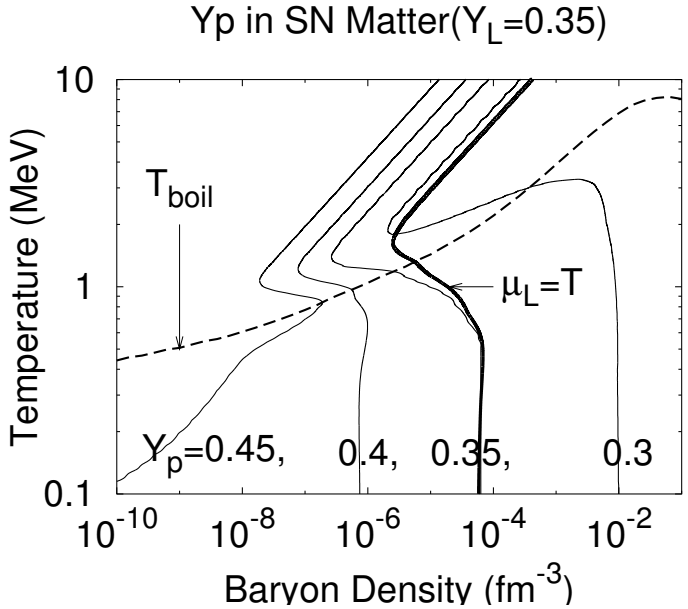

Fig. 12. Proton fraction contours in supernova matter at $Y_L = 0.35$ calculated in NSE. Thin solid lines show contours at $Y_p = 0.45, 0.40, 0.35$ and 0.30. Thick solid line shows the trapping density ρ_{trap} at which the condition $\mu_L = T$ is satisfied. (The contour $Y_p = Y_e = 0.35$ corresponds to $\mu_L = 0$.) The boiling temperature is shown by dashed line.

evolution. The second point is the yield of heavy unstable fragments at the ν-sphere: If short lived unstable fragments are abundantly formed, they decay quickly and modify the proton fraction outside the ν-sphere. The third is the fragment distribution at given Y_p values instead of Y_L.

First, we consider the β-equilibrium condition in supernova matter. In Fig. 12, we show the trapping density ρ_{trap} at which $\mu_L = T$ is satisfied, and the proton fraction in the fixed-Y_L supernova matter. As discussed before, ρ_{trap} approximately corresponds to the ν-sphere. While nuclear matter is more symmetric at higher temperature (and at higher entropy) in general, the isospin symmetrization is strong in the coexisting region then larger proton fractions would appear especially around the boiling temperature. Consequently when the supernova matter experiences the phase transition inside the ν-sphere, the proton fraction is limited to $Y_p \gtrsim 0.33$ for $Y_L = 0.35$ later on.

We also find that the trapping density at the boiling temperature is around $10^{-5}\mathrm{fm}^{-3}$. At this density, nuclei at around the first peak of r-process ($N \sim 50$) are abundantly formed as seen in Fig. 10. Although these nuclei are often very neutron rich (Fig. 11), the life-times ($\gtrsim$ 100 msec) are still longer than the dynamical expansion time scale ($\sim$ 1 msec). Thus until the matter reaches the charged particle reaction freeze-out temperature, constant Y_p evolution would be expected.

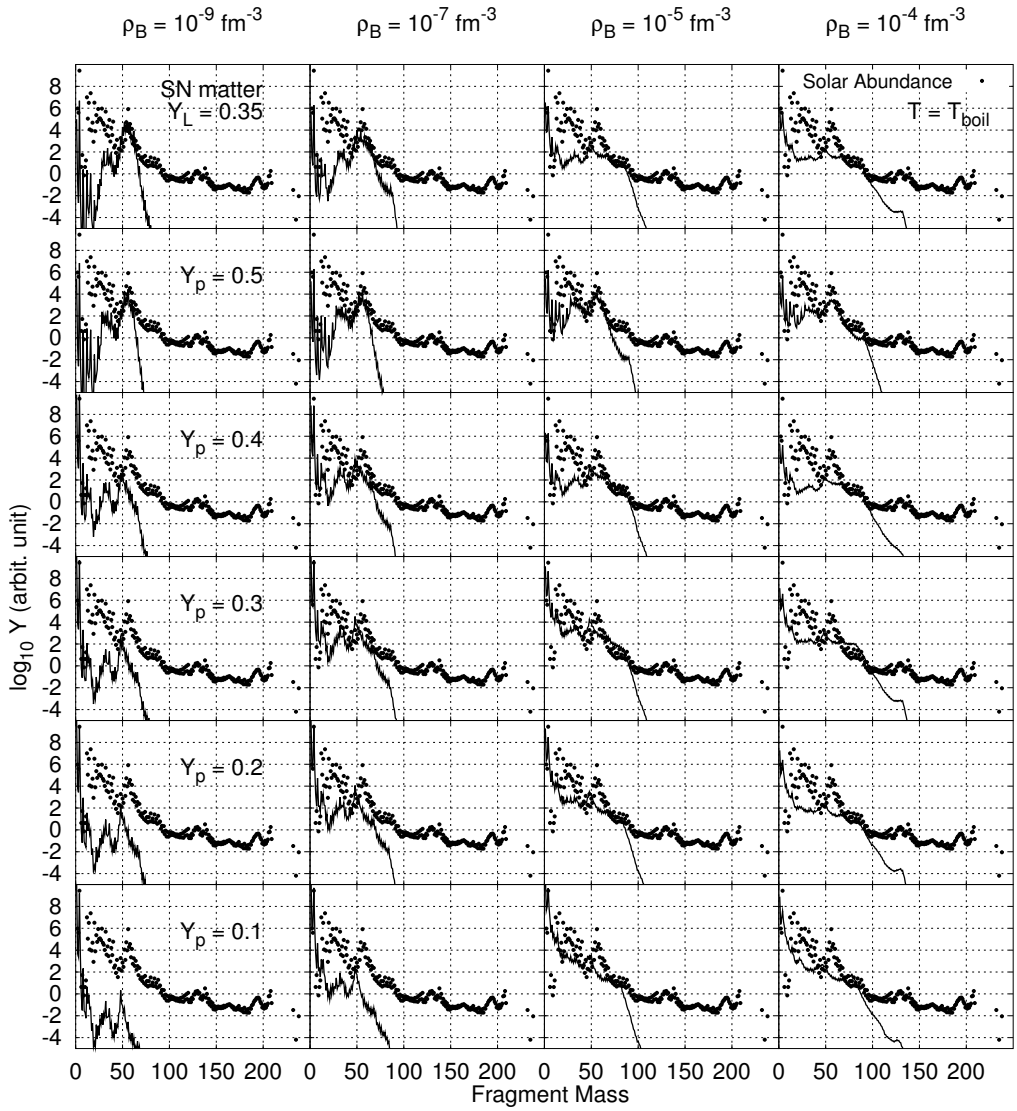

Fig. 13. The fragment distribution in supernova matter with $Y_p = 0.5, 0.4, 0.3, 0.2, 0.1$ (thick lines, constituents $= n, p, e^-$ and their antiparticles) and supernova matter with $Y_L = 0.35$(thin lines, constituents $= n, p, e^-, \nu_e, \gamma$ and their antiparticles) at the boiling points for each $\rho_B = 10^{-9}, 10^{-7}, 10^{-5}, 10^{-4}$ fm^{-3} in comparison with the solar abundance (filled circles).

Next, we show in Fig. 13 the mass distribution in supernova matter with fixed Y_p at the boiling point for densities from 10^{-9} to 10^{-4} fm^{-3} in comparison with the distribution in supernova matter with $Y_L = 0.35$ (top panel). Here the boiling points of supernova matter at fixed Y_p are summarized in Table. 2. For constant Y_p, T_{boil} is defined by the peak of M_2/M_1 [7], since there appear two peaks in ξ' contrary to the case of constant Y_L.

The first column shows the result at $\rho_B = 10^{-9}$ fm^{-3}. In the case of $Y_p = 0.5$, we can observe a large amount of nuclei around mass number $A \sim 30$ and their

Table 2
Boiling points of neutrino-less supernova matter in NSE as a function of the baryon density and proton fraction Y_p. Results with Coulomb corrections are shown.

	The boiling temperature (MeV)						
$\rho_B(\mathrm{fm}^{-3})$	10^{-10}	10^{-9}	10^{-8}	10^{-7}	10^{-6}	10^{-5}	10^{-4}
$Y_p = 0.1$	0.52	0.60	0.70	0.86	1.09	1.47	2.20
0.2	0.52	0.60	0.71	0.86	1.10	1.49	2.25
0.3	0.52	0.60	0.71	0.86	1.10	1.49	2.23
0.4	0.52	0.60	0.70	0.84	1.05	1.40	2.10
0.5	0.46	0.52	0.61	0.73	0.90	1.16	1.68

yields are not negligible compared to the iron peak nuclei. At $Y_p \leq 0.4$, we can see the two peak structures around mass number A = 30 and A= 50 in addition to the light nuclei. Similar trend can be seen at $\rho_B = 10^{-7}$ fm^{-3} as shown in the second column of Fig. 13. In addition, heavy nuclei around the first r-process peak are formed in the tail region of the mass distribution.

At these very low densities, the seed-nuclei of the r-process would be obtained after the freeze-out of charged particle reactions. In previous works on supernova r-process [10–14], the network calculations are made to start from NSE abundance pattern rather than from one dominant configuration. Our results suggest the necessity to take account of the distribution at $T = T_{boil}$. It also applies to lower temperatures than T_{boil}. Below T_{boil}, we can still see two peak structure in the mass distribution (not shown here) as in the case of $T = T_{boil}$. Therefore, it is expected that fragment distribution would have some effects on later r-process. This finding supports the idea to use NSE distribution adopted in the above works [10–14]. In addition, it would be dangerous to start the network calculation at around T_{boil}, because the fragment yield in the initial condition is very sensitive to the small difference in T.

At higher densities around the surface of the ν-sphere ($\rho_B = 10^{-4}$ and 10^{-5} fm^{-3}, shown in the third and fourth columns), the distributions resembles to that under β-equilibrium (top panel). At these densities, various nuclei up to the first r-process peak ($A \sim 80$) are abundantly formed independently to whether neutrinos are trapped or not.

4.2 Possible relation to supernova nucleosynthesis

The present model calculation suggests that adiabatic paths of dense matter go across the boundary of coexisting region, then the material would go through the coexisting region during the expansion. Next question, then, is

whether the elements made through the liquid-gas phase transition are ejected to outside. If they are ejected, they contribute to the following nucleosynthesis of heavy elements such as the r-process, because various nuclei up to the first r-process peak might be already synthesized at equilibrium. Although the ejection of matter is not warranted and non-equilibrium effect is not negligible, it is worth trying to discuss outcome of fragment distribution we found in a context of hydrodynamical calculation of supernova matter.

In order to examine this possibility, we analyse the results of hydrodynamical calculation of core-collapse supernova [24]. In that work, the EoS table derived by the RMF-TF model with the TM1 interaction [17] has been used in the general relativistic hydrodynamics [31]. Note that this EoS table and the EoS in NSE give almost the same pressure as shown in Fig. 9. Among series of model calculations of adiabatic collapse, a case of iron core of $15M_\odot$ presupernova star [32] explode hydrodynamically with fixed electron fractions, which were assumed to study the properties of EoS in a model explosion. In this model explosion, the material from deep inside the core is ejected. The entropy per baryon of this ejecta is about $S/B \sim 10$ determined by the shock passage. The trajectory of this ejecta passes through the coexisting region. Further inner material has lower entropies down to $S/B \sim 1$, which are favorable for the heavy element production through liquid-gas phase transition, but the ejection becomes rather difficult. At around $S/B \sim 10$, it has been shown that successful r-process nucleosynthesis can be described in the case of model explosion from a presupernova star of $11M_\odot$ with a small iron core by the dynamical ejection of neutron-rich material [33]. Although hydrodynamical explosion (so-called prompt explosion) has been claimed to be limited for very small iron core, extreme cases of EoS, and electron capture rates [8,9], the outcome of nucleosynthesis is extremely interesting if the mass ejection really occurs.

If the materials are ejected from deep inside, these ejecta should experience the liquid-gas phase transition before ejection. If the ejection from relatively high density ($\rho_B \geq 10^{-5}$ fm^{-3}) takes place, the formed fragments are generally very neutron rich as shown in Fig. 11 and some part of them are unstable against neutron emission. These nuclei provide a huge amount of neutrons, which would help the following r-process to proceed up to heavier r-process elements around actinides.

Strictly speaking, these direct contributions to nucleosythesis should be discussed with proton fractions at freeze-out points determined by the hydrodynamical evolution outside ν-sphere, where we need to take account of compositional change and neutrino transport. It should be noted that the model explosion in Ref. [24] is obtained in a simplified calculation without neutrino-transport assuming large electron fractions. Since successful explosion by simulations of hydrodynamics with neutrino-transport has not yet

been shown, the condition of (ρ_B, T, Y_e), fragmentation of ejecta, and following nucleosynthesis (including the r-process) is still an open question.

5 Summary and discussion

In this paper, we have investigated the liquid-gas phase transition of supernova matter, and its effects on the fragment formation by using two models — the Relativistic Mean Field (RMF) model and the Nuclear Statistical Equilibrium (NSE) model.

In RMF, we have used the interaction TM1, which has been successfully applied to finite nuclei including neutron rich unstable nuclei, neutron stars, and supernova explosion [17,26–28]. Leptons are shown to play non-trivial roles such as the symmetrization of nuclear part of supernova matter. As a result, nuclear liquid gains symmetry energy, and the calculated boiling points in supernova matter ($T_{boil} > 1$ MeV for $\rho_B \geq 10^{-10}$ fm^{-3}) are comparable to those in symmetric nuclear matter at low densities. Adiabatic paths are shown to go across the boundary of coexisting region. Clear concentration of adiabatic paths to the boundary of coexisting region have been found. All of these findings suggest that at least a part of ejecta in supernova explosion would experience the liquid-gas phase transition before freeze-out.

In NSE, we have adopted the mass table of around 9000 nuclei constructed by Myers and Swiatecki [30], since larger species of nuclei become stable with the Coulomb energy correction due to electron screening as a medium effect [16]. Because of the finiteness of nuclei, they lose surface and Coulomb energy compared to the case of coexistence treatment of two infinite matter phases in RMF. The boiling points become slightly lower, but they are still high; $T_{boil} \geq 0.5$ MeV for $\rho_B \geq 10^{-9}$ fm^{-3}. Calculated fragment mass distributions around $T_{boil}(\rho_B)$ show enhancement of the first, second, and third peak r-process elements at $\rho_B = 10^{-5}, 10^{-3}$, and 10^{-2} fm^{-3}, respectively. These (ρ_B, T) conditions are still inside the ν-sphere. In addition, calculated isotope distribution shows that very neutron rich nuclei around and beyond the neutron dripline may exist under thermal and chemical equilibrium in supernova matter with degenerate neutrinos.

Calculated results in this work support several aspects of the standard treatment of supernova matter: The equation of state (EoS) in NSE is very similar to that in the Thomas-Fermi treatment, where only one dominant configurations is considered, and the main products in NSE are shown to be n, p, α, and iron peak nuclei at low densities outside the ν-sphere, where the calculations are carried out with fixed Y_p. This may be because the EoS and main products are determined by the average multiplicity of fragments and the binding

energy. On the other hand, we cannot neglect the fragment distribution effects at $T \lesssim T_{boil}$ shown for the plausible Y_p values in the processes in which the importance for each species of nuclei is very different. For example, the abundance pattern in the liquid-gas coexisting region will have some influences on the later r-process as the seed element distribution. Nuclear reactions involving neutrinos would be affected as well; the electron capture process is very sensitive to the mass number and shell effects of nuclei, and neutrino-nucleus scattering cross section is proportional to A^2 rather than A [37].

In this work, we have assumed equilibrium throughout this paper. One of the key questions is the freeze-out conditions of supernova matter, at which nuclear reactions become less frequent and supernova matter goes off equilibrium in the expansion time-scale. The seed element distribution of the r-process will be given as the nuclear distribution on the freeze-out line in the (ρ_B, T) diagram. It is important to determine the freeze-out condition in supernova dynamics. Another important direction is to construct a model which includes both of the mean field nature such as in RMF and the statistical nature in NSE. In a present NSE treatment, only the Coulomb correction is included as the medium effects, and medium effects from strong interactions are neglected. This neglection may lead to the overestimate of neutron rich nuclei, as discussed in recent statistical fragmentation models [38]. On the other hand, in the Thomas-Fermi treatment of heavy-nuclei with EoS derived using RMF, since statistical nature or fragment distribution is not taken care of at around T_{boil}, the treatment is not sufficient. Works in these directions are in progress.

Acknowledgments

The authors are grateful to Prof. K. Kato, Dr. M. Ito and Dr. K. Iida for useful discussions and suggestions. This work was supported in part by the Grant-in-Aid for Scientific Research (Nos. 09640329 and 13740165) from the Ministry of Education, Science and Culture, Japan.

A Low Density Approximation

In the calculation of liquid-gas coexistence at low temperatures, it becomes necessary to solve the chemical equilibrium of liquid and very low density gas. For example, the gas baryon density becomes around $\rho_B^{Gas} = 10^{-74}$ fm^{-3} at the coexisting condition $(\rho_B, T) = (10^{-10}\text{ fm}^{-3}, 0.1\text{MeV})$. In order to efficiently obtain the derivative matrix $\partial\mu_i/\partial\rho_j$ $(i, j = B, C, L)$, which are required in solving coexistence, we take the low temperature and low density approximation for nucleons at low baryon densities ($\rho_B \ll 10^{-5}$ fm^{-3}) around and below the boiling point in the mean field calculation.

In the mean field approximation, nucleon distribution is a function of the effective mass $M^* = M + g_\sigma\sigma_0$ and effective chemical potentials $\nu_i = \mu_i - g_\omega\omega_0 - g_\rho\tau_i\rho_{30}$ ($i = n$ or p), where σ_0, ω_0 and ρ_{30} are the expectation values of the meson fields of σ, ω and the neutral ρ mesons, respectively. For a given baryon density ρ_B and proton fraction Y_p, the vector meson expectation values are uniquely determined as $\omega_0 = \omega_0(\rho_B), \rho_{30} = \rho_{30}(\rho_T)$, where $\rho_T \equiv \rho_p - \rho_n$. In a non-relativistic limit [22], we can take energy as $E^* = M^* + p^2/2M^*$. At low densities $\left(\rho_B \ll 10^{-5}\text{ fm}^{-3}\right)$, the nucleon fugacity $f_i \equiv \exp\left(-(M_i^* - \nu_i)/T\right)$ becomes much smaller than unity, then we can safely ignore the second and higher order terms in the fugacity f_i. In this approximation, the Fermi distribution is approximated to be the Boltzmann distribution, then the baryon number density ρ_i and the scalar density ρ_s are analytically obtained for a given value of σ_0 as,

$$\rho_i(\nu_i, \sigma_0) = G_-(\nu_i, M^*(\sigma_0), T) + O(f_i^2)\ , \tag{A.1}$$

$$\rho_s(\nu_n, \nu_p, \sigma_0) = G_+(\nu_n, M^*(\sigma_0), T) + G_+(\nu_p, M^*(\sigma_0), T) + O(f^2)\ , \tag{A.2}$$

$$G_\pm(\nu, M^*, T) = g\left(\frac{M^*T}{2\pi\hbar^2}\right)^{\frac{3}{2}}\left(e^{\nu/T} \pm e^{-\nu/T}\right)e^{-M^*/T}\ . \tag{A.3}$$

The self-consistent condition $\sigma_0 = \sigma_0(\rho_s(\nu_n, \nu_p, \sigma_0))$ can be solved by iteration using (A.1-A.3), which converges in a few steps at low densities. All of the above densities are represented by three variables, ν_n, ν_p and σ_0 for a given temperature T, and we can eliminate the σ_0 dependence by using the total derivative of the above self-consistent condition.

$$d\sigma_0 = \frac{d\sigma_0}{d\rho_s}\left(\frac{\partial\rho_s}{\partial\nu_n}\,d\nu_n + \frac{\partial\rho_s}{\partial\nu_p}\,d\nu_p + \frac{\partial\rho_s}{\partial\sigma_0}\,d\sigma_0\right)\ , \tag{A.4}$$

$$d\rho_i = \frac{\partial\rho_i}{\partial\nu_i}\,d\nu_i + \frac{\partial\rho_p}{\partial\sigma_0}d\sigma_0\ , \tag{A.5}$$

$$d\mu_i = d\nu_i + g_\omega\frac{d\omega_0}{d\rho_B}\,d\rho_B + g_\rho\tau_i\frac{d\rho_{30}}{d\rho_T}\,d\rho_T\ . \tag{A.6}$$

By solving the first equation (A.4) in $d\sigma_0$ and substituting it in the second equation (A.5), we obtain $\partial\rho_i/\partial\nu_j$ and then $\partial\nu_i/\partial\rho_j$. Finally, the third equation (A.6) gives the partial derivatives $\partial\mu_i/\partial\rho_j$ by eliminating $d\nu$. Having the (relativistic) lepton integrals and the above derivatives in nucleons, it is straightforward to construct the matrix $\partial\mu_i/\partial\rho_j$ $(i,j = B,C,L)$.

B Procedures to obtain coexisting region of supernova matter in RMF

The boundary of coexisting region of supernova matter has been determined in three steps; symmetric nuclear matter, asymmetric nuclear matter, and supernova matter.

First, for a given temperature, we solve the coexisting condition in symmetric nuclear matter ($Y_p^{Liq.} = Y_p^{Gas} = 0.5$). If there is a density region where pressure is decreasing for increasing ρ_B, liquid and gas phases can coexist, and we can find coexisting densities, $\rho_B^{Liq.}$ and ρ_B^{Gas}, by using the Maxwell construction. Secondly, we solve the coexisting condition for $(\rho_B^{Liq.}, Y_p^{Liq.})$ and $(\rho_B^{Gas}, Y_p^{Gas})$ in asymmetric nuclear matter. Having the coexisting condition at a given $Y_p^{Liq.}$, it is easy to find coexisting condition for slightly different $Y_p^{Liq.}$ by using the multi-dimensional Newton's method. Starting from symmetric nuclear matter, three variables $(\rho_B^{Liq.}, \rho_B^{Gas}, Y_p^{Gas})$ are determined for a given $Y_p^{Liq.}$ which is slightly different from that in the previously solved condition by requiring the condition, $\mu_B^{Liq.} = \mu_B^{Gas}$, $\mu_C^{Liq.} = \mu_C^{Gas}$, and $P^{Liq.} = P^{Gas}$. We show the boundary of coexisting region of (ρ_B, Y_p) by the thick solid line in Fig. B.1. Filled circles show the point where two phase become uniform, $(\rho_B^{Liq.}, Y_p^{Liq.}) = (\rho_B^{Gas}, Y_p^{Gas})$. The density gap $\rho_B^{Liq.} - \rho_B^{Gas}$ generally decreases as the liquid becomes more asymmetric, because of the symmetry energy loss. At lower temperature, the coexisting pressure and thus the coexisting gas baryon density become small, then larger density gap appears. Thirdly, proton fraction Y_p is determined as a function of ρ_B in uniform (homogeneous) supernova matter at a given Y_L, by using the charge neutrality condition, $\rho_e = \rho_p = Y_p\rho_B$, and the chemical equilibrium condition, $\mu_\nu = \mu_L = \mu_e + \mu_p - \mu_n$. When Y_p is in the coexisting region of nuclear matter, liquid and gas phases can coexist in supernova matter. The boundary of coexisting region for a given T is determined by the crossing point of these two lines. Since Y_p becomes smaller for smaller Y_L as shown in Fig. B.1, the coexisting density region becomes narrower for smaller Y_L. This is the reason why the boiling temperatures decrease for smaller lepton fraction as shown in Fig. 1.

For neutrino-less supernova matter (NS), the procedure is almost the same, except that the chemical equilibrium condition is modified to $\mu_\nu = 0$.

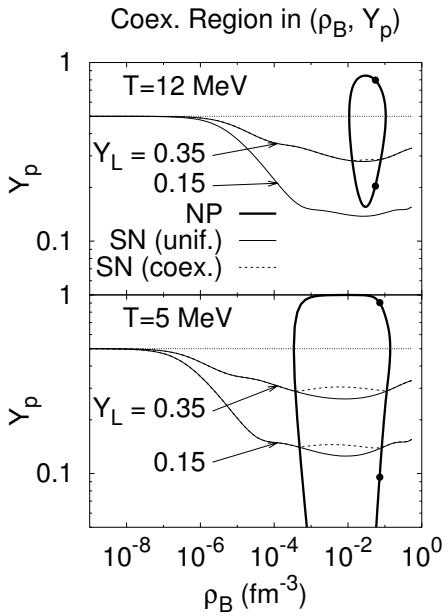

Fig. B.1. The boundary of liquid-gas coexisting region in nuclear matter (thick solid lines), and proton fraction as a function of the baryon density in supernova matter without (thin solid lines) and with (dotted line) coexistence. Filled circles show the points where liquid and gas phases converges to the uniform matter.

References

[1] J. Pochodzalla et al. (ALADIN Collab.), Phys. Rev. Lett. **75** (1995), 1040;
V. Serfling et al. (ALADIN Collab.), Phys. Rev. Lett. **80** (1998), 3928;
W. Reisdorf et al. (FOPI Collab.), Nucl. Phys. **A612** (1997), 493;
B. Borderie et al. (INDRA Collab.), Phys. Rev. Lett. **86** (2001), 3252;
M. D'Agostino et al., Phys. Lett. **B473** (2000), 219;
B. K. Srivastava et. al. (EOS Collab.), Phys. Rev. C **65** (2002), 054617;
H.S. Xu et al., Phys. Rev. Lett. **85**(2000), 716.

[2] M. E. Fisher, Physics **3** (1967), 255; Rep. Prog. Phys. **30** (1967), 615.

[3] J. Aichelin, Phys. Rep. **202** (1991), 233;
A. Ono, H. Horiuchi, T. Maruyama, A. Ohnishi, Prog. Theor. Phys. **87** (1992), 1185;
H. Feldmeier, J. Schnack, Prog. Part. Nucl. Phys. **39** (1997), 393;
A. Ohnishi, J. Randrup, Phys. Lett. **B394** (1997), 260;
A. Ono, Phys. Rev. C **59** (1999), 853;
S. Chikazumi, T. Maruyama, S. Chiba, K. Niita, A. Iwamoto, Phys. Rev. C **63** (2001), 024602.

[4] D. H. E. Gross, Rept. Prog. Phys. **53** (1990), 605;
J.P. Bondorf, A.S. Botvina, A.S. Ilinov, I.N. Mishustin, K. Sneppen, Phys. Rep. **257**(1995), 133;
L.G. Moretto, G.J. Wozniak, Ann. Rev. Nucl. Part. Sci. **43** (1993), 379;

S. Pratt, S. Das Gupta, Phys. Rev. C **62**(2000), 044603;
A.S. Parvan, V.D. Toneev, M. Ploszajczak Nucl. Phys. **A676**(2000), 409.

[5] Y. Hirata, A. Ohnishi, Y. Nara, T. Kido, T. Maruyama, N. Otuka, K. Niita, H. Takada, S. Chiba, Nucl. Phys. **A** (2002), in press; Eprint: nucl-th/0111019.

[6] G. Fai and J. Randrup, Nucl. Phys. **A381** (1982), 557.

[7] W. Bauer, Phys. Rev. **C38** (1988), 1297.

[8] H. A. Bethe, Rev. Mod. Phys. **62** (1990), 801.

[9] H. Suzuki, Physics and Astrophysics of Neutrinos, edited by M. Fukugita and A. Suzuki, (Springer-Verlag, Tokyo, 1994), p.763.

[10] E. M. Burbidge, G. R. Burbidge, W. A. Fowler and F. Hoyle, Rev. Mod. Phys. **29** (1957), 547.

[11] B. S. Meyer, Ann. Rev. Astron. Astrophys. **32** (1994), 153.

[12] W. Hillebrandt et al. Astron. Astrophys. **52** (1976), 63.

[13] S. E. Woosley et al. Astrophys. J **433** (1994), 229.

[14] K. Takahashi et al. Astron. Astrophys. **286** (1994), 857.

[15] K. Lamb High Energy Astrophysics, The Benjamin Cummings Publishig Company, Inc.

[16] D. Q. Lamb, J. M. Lattimer, C. J. Petheck and D. G. Ravenhall, Nucl. Phys. **A360** (1981), 459, and references therein.

[17] H. Shen, H. Toki, K. Oyamastu and K. Sumiyoshi, Prog. Theor. Phys. **100** (1998), 1013; Nucl. Phys. **A637** (1998), 435.

[18] J. M. Lattimer and F. D. Swesty, Nucl. Phys. **A535** (1991), 331.

[19] C. Ishizuka, A. Ohnishi, K. Sumiyoshi, Proc. of the Yukawa International Seminar 2001 on Physics of Unstable Nuclei (YKIS01), Prog. Theor. Phys. Suppl. (2002), in press.

[20] B. D. Serot and J. D. Walecka, Adv. Nucl. Phys. **16** (1986), 1.

[21] Y. Sugahara, H. Toki, Nucl. Phys. **A579** (1994), 557.

[22] H. Müller and B. D. Serot, Phys. Rev. **C52** (1995), 2072.

[23] P.K. Sahu, A. Ohnishi, Prog. Theor. Phys. **104**(2000), 1163;
M. Malheiro, A. Delfino, C. T. Coelho, Phys. Rev. **C58** (1998), 426;
W. L. Qian, R. K. Su, Phys. Lett. **B491**(2000), 90;
A. Sedrakian, Phys. Rev. **C63** (2001), 025801.

[24] K. Sumiyoshi, H. Suzuki, S. Yamada and H. Toki, submitted to Nucl. Phys. **A** (2001).

[25] E. Anders and N. Grevesse, Geochim. Cosmochim. Acta **53** (1989), 197.

[26] K. Sumiyoshi, H. Kuwabara and H. Toki, Nucl. Phys. **A581** (1995), 725.

[27] K. Sumiyoshi, H. Suzuki, K. Otsuki, M. Terasawa and S. Yamada, Pub. Astron. soc. Japan **52** (2000), 601.

[28] K. Sumiyoshi, H. Suzuki and H. Toki, Astron. Astrophys. **303** (1995), 475.

[29] D. D. Clayton, in "Principles of Steller Evolution and Nucleosynthesis" The University of Chicago Press (1983).

[30] W. D. Myers and W. J. Swiatecki, LBL-36803 (1994); Ann. of Phys. **204** (1990), 401.

[31] S. Yamada, Astrophys. J. **475** (1997), 720.

[32] S. E. Woosley and T. Weaver, Astrophys. J. Suppl. **101** (1995), 181.

[33] K. Sumiyoshi, M. Terasawa, G.J. Mathews, T. Kajino, S. Yamada, and H. Suzuki, Astrophys. J. **562** (2001), 880.

[34] H. T. Janka, K. Kifonidis and M. Rampp, Proc. Workshop on Physics of Neutron Star Interiors (ECT*, Trento, June 19-July 7, 2000), ed. D. Blaschke, N.K. Glendenning, A.D. Sedrakian, Springer, in press; Lect.Notes Phys. 578 (2001), 333-363; astro-ph/0103015.

[35] T. Shimizu, S. Yamada and K. Sato, Astrophys. J. **432** (1994), L119.

[36] A. I. MacFadyen and S.E. Woosley, Astrophys. J. **524** (1999), 289.

[37] C. Ishizuka, A. Ohinishi, K. Sumiyoshi in preparation.

[38] S. Ray, J. Shamanna, T. T. S. Kuo, Phys. Lett. **B392** (1997), 7;
P. Chomaz, F. Gulminelli, Phys. Lett. **B447**(1999),221;
V. Baran, M. Colonna, M. Di Toro, V. Greco, M. Zielinska-Pfabe, H.H. Wolter, Nucl. Phys. **A703** (2002), 603.